Predicting droplet vibration in oil subjected to chaotic pulse group electric field excitation using LSTM

Ye Peng[1], Yaozhong Hu*[2], Haifeng Gong[3], Lin Yan[2], Bao Yu[3], Hong Yin[2], Ping Ouyang[2]

[1]School of Mechanical Engineering, Chongqing Technology and Business University, Chongqing, 400072, China
[2] Engineering Research Centre for Waste Oil Recovery Technology and Equipment of Ministry of Education, Chongqing Technology and Business University, Chongqing, 400072, China
[3] School of Environment and Resources, Chongqing Technology and Business University, Chongqing, 400072, China

Abstract: Oil-water separation is the key step in the process of converting waste oil into a resource.The chaotic pulse group (CPG) electric field is now regarded as an emerging method for oil-water separation.However, droplet vibration under CPG electric field excitation involves complex parameters that are challenging to analyze. Traditional numerical methods are hampered by high computational demands, lengthy processing times, and limited output, restricting further exploration of vibration characteristics. To address these limitations, this paper proposes a prediction model for droplet vibration under CPG electric field excitation using a long short-term memory (LSTM) neural network. The research results show that the LSTM model can effectively extract and learn the long-term dependencies in the droplet vibration sequence, capture the relationship between droplet vibration and chaotic pulse group electric field signals as well as time, thereby achieving accurate predictions and saving computing resources. Moreover, the LSTM model outperforms BP, GRU, and CNN models on the test set in terms of prediction accuracy.

1 Introduction

During the use of lubricating oil, it may be contaminated by impurities such as water, resulting in industrial waste oil[1]. If not properly disposed of, it will not only lead to waste of resources but also cause environmental pollution. Therefore, the resource utilization of waste oil is of great significance[2,3]. In the process of converting waste oil into resources, oil-water separation is the key step. The common methods for oil-water separation include sedimentation, centrifugation, membrane separation, microwave demulsification, chemical demulsification, biological demulsification, ultrasonic demulsification and electrostatic method[4,5]. The electric field method, in particular, employs a high-voltage electric field to induce droplet deformation and vibration, weakening the interfacial film and increasing collision likelihood, thus achieving efficient oil-water separation. This approach is widely used in industrial demulsification due to its environmentally friendly and efficient nature[6,7].

Common electric fields in the electric field method include direct current, alternating current, and pulsed electric fields[8]. Among diverse processing methods, the pulsed electric field strategy has drawn substantial attention from researchers, as it features low energy consumption and high efficiency[9]. Li et al. demonstrated experimentally that there is an optimal demulsification frequency at which droplet oscillation and deformation are maximized, making polarization coalescence most pronounced[10]. Zhang Jian[11] analyzed the forces on droplets in emulsions under an electric field and established a formula for the natural frequency of droplet oscillation in W/O emulsions. He also provided a mechanical explanation for the optimal frequency and derived its calculation formula. These studies have demonstrated that the optimal demulsification frequency has a significant impact on the polarization of droplets. However, as droplet size changes dynamically during demulsification, the optimal demulsification frequency also varies, complicating the adaptation of a single-frequency pulsed electric field. To address this, a chaotic pulse group electric field was proposed for demulsification and dehydration, leveraging its frequency variation to match changes in the optimal demulsification frequency[12]. Currently, research on chaotic pulse group electric fields for demulsification and dehydration is in its early stages. The finite element numerical method is commonly used to study droplet dynamics under electric field excitation. However, for studying droplet vibration in oil under chaotic electric field excitation, this method involves complex parameters, demands significant computing resources, and yields limited data, hindering deeper research. Thus, enhancing computing speed and resource efficiency has become a key research focus in this field.

Recently, deep learning strategies represented by neural networks have manifested considerable potential in the numerical characterization and analysis of two-phase flows. These methods bypass the need to explicitly solve

*Corresponding author: hyztzx@163.com

the complex equations governing phase interface evolution and multi-field coupling in two-phase flows. Instead, they directly establish complex nonlinear mappings between inputs—such as flow field parameters, physical properties, and boundary conditions—and key outputs like phase distribution, phase velocity, and interface deformation. This approach enables rapid and accurate predictions of flow field evolution and core characteristics of two-phase flows. It is particularly suitable for engineering simulations of two-phase flow systems with high variable dimensions, complex phase interface behaviors, unclear multi-phase coupling mechanisms, and ample experimental and simulation data. This method offers a novel solution to the bottlenecks of traditional numerical methods regarding computational efficiency and the accuracy of complex interface capture. Asadolahpour et al. proposed a deep learning workflow using a high-dimensional Vision Transformer (HD-ViT) for predicting phase distribution in pore-scale two-phase flow. By utilizing sub-samples of rock CT images and input features like pixel size, interfacial tension, contact angle, and pressure, a large-scale dataset is generated through a pore morphology simulator for training. This model exhibits remarkable accuracy and speed advantages on images of various rock types, such as sandstone and carbonate rocks. It can produce results comparable to experiments and lattice Boltzmann simulations within seconds and has been effectively extended to 3D applications, offering an efficient solution for studying two-phase flow in porous media[13]. Xiao et al. constructed a three-dimensional instantaneous particle volume fraction (PVF) field reconstruction model based on deep learning, aiming to address the difficulty in acquiring the PVF field of solid-liquid two-phase flow in vertical lifters for deep-sea mining. This model adopts a two-stage structure, integrating an upsampling module with an improved autoencoder that incorporates skip connections and a multi-head cross-attention mechanism. It can accurately reconstruct the global PVF field using single-section data. Under standard operating conditions, the model achieves a coefficient of determination (R^2) of 0.962 and a mean square error (MSE) of 3.98×10^{-15}. Even when the input cross-sectional position varies, strong noise interference exists, and the pipe length is extended to 50 times the pipe diameter, the model still maintains stable performance. By virtue of transfer learning, it can rapidly adapt to new particle concentration conditions with only 10% of the training samples[14]. Siriwardana et al. established a machine learning framework utilizing 10,300 groups of experimental data, which integrates decision tree ensembles, support vector machines, and various neural network architectures for the multi-classification identification of seven two-phase flow patterns: circular flow, bubble flow, churn flow, dispersed flow, intermittent flow, laminar smooth flow, and wavy flow. By employing oversampling to address data imbalance and using Bayesian optimization for hyperparameter tuning, the results indicate that the lightweight gradient enhancer (LightGBM) achieves the highest classification accuracy of 98.9%[15].

To tackle the aforementioned issues, this paper presents a droplet vibration prediction model in oil, utilizing LSTM, under chaotic electric field excitation. The model effectively captures the long-term dependencies in the nonlinear vibration of droplets, enabling precise prediction of droplet vibration.

2 Methods

2.1 Long Short-Term Memory Neural Network

As a specialized variant of recurrent neural networks (RNNs), long short-term memory (LSTM) neural networks are proposed to tackle the inherent problems present in long time-series data processing. In RNNs, the weight matrix is updated internally using the backpropagation algorithm, while the gradient propagates among these weight matrices. However, when the time series extends beyond a certain length, problems like gradient explosion or vanishing gradients can arise. These problems lead the model to lose track of earlier temporal information, which in turn degrades the precision of predictive outcomes. As a solution to such limitations, the long short-term memory (LSTM) model was consequently proposed[16]. The LSTM model effectively retains time series information over extended periods using its memory units and gating structures. As depicted in Figure 1, the LSTM model primarily comprises a memory unit and three gate control units: the input gate, forget gate, and output gate. The input gate regulates the amount of state information preserved at the current time while incorporating new information. The forget gate determines the extent of previously stored state information to discard, thereby maintaining long-term dependencies. The output gate manages the amount of state information released at the current time. The memory unit not only preserves both short-term and long-term dependencies within the time steps but also updates information via the gate control units.The calculation formula under the time step t is as shown in equations (1)-(6)[17]:

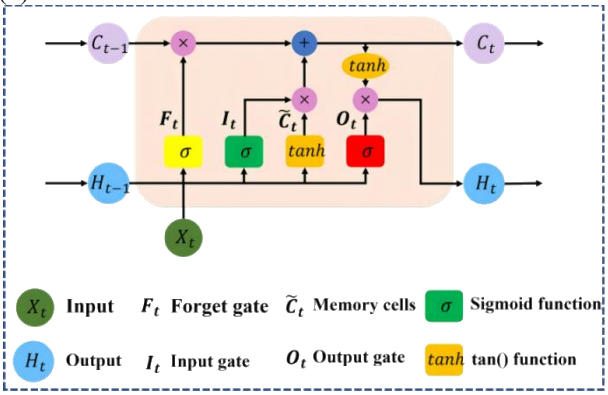

Figure 1 Structure of LSTM Unit

$$I_t=\sigma(X_tU_i+H_{t-1}N_i+b_i) \quad (1)$$
$$F_t=\sigma(X_tU_f+H_{t-1}N_f+b_f) \quad (2)$$
$$O_t=\sigma(X_tU_o+H_{t-1}N_o+b_o) \quad (3)$$
$$\tilde{C}_t=tanh(X_tU_c+H_{t-1}N_c+b_c) \quad (4)$$
$$C_t=F_tC_{t-1}+I_t\tilde{C}_t \quad (5)$$
$$H_t=O_t\,tanh(C_t) \quad (6)$$

In the formula, σ denotes the sigmoid function, which indicates a value range of [0,1]. X_t represents the input at the current time step, while H_{t-1} signifies the hidden state at time step t-1. C_t refers to the current state of the memory cell, and the $tanh(\cdot)$ function ensures that the hidden state value remains between -1 and 1. $I_t, F_t, O_t, \widetilde{C}_t$ stands for the input gate, forgetting gate, output gate, and memory cell. U is the state-input parameter matrix, and N is the state-state parameter matrix, which includes the deviation parameter.

2.2 Model Structure

The LSTM model presented in this paper employs a modular serial structure, illustrated in Figure 2. This architecture sequentially consists of an input layer, an LSTM layer, an attention mechanism layer, a fully connected layer, and an output layer. The input layer receives and normalizes preprocessed time series data. Serving as the core feature extraction unit, the LSTM layer identifies long-term dependencies within the sequence data. The attention layer highlights key temporal features by adaptively distributing weights and suppressing redundant information. The fully connected layer integrates and applies nonlinear mapping to the extracted high-dimensional features. Finally, the output layer generates the task-related predictive output. Given the limited parameters of droplet vibration under chaotic pulse group excitation, this study uses the chaotic pulse group signal and time as model inputs, with droplet vibration as the model output.

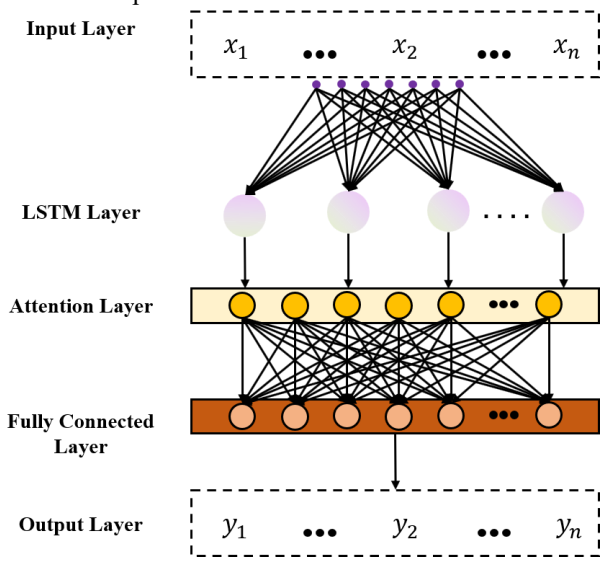

Figure 2 Model Framework

2.3 Data Preprocessing and Evaluation indicators

2.3.1 Data Preprocessing

To improve the model's predictive performance, data standardization is essential. This process involves scaling all features of the time series data to a uniform dimension, which prevents variations in data dimensions from affecting the model's accuracy. Additionally, standardizing the data can speed up the model's prediction process. Typically, this is achieved through the min-max standardization method. The calculation formula is as follows:

$$X_i=\frac{x_i-x_{min}}{x_{max}-x_{min}} \tag{7}$$

In the formula, X_i denotes the standardized data, x_i signifies the initial data, x_{min} indicates the minimum value within the initial data, and x_{max} represents the maximum value within the initial data.

2.3.2 Evaluation Indicators

To assess the model's predictive performance, three indicators are employed: mean absolute error (MAE), mean square error (MSE), and coefficient of determination(R^2). Both MAE and MSE measure the overall error magnitude between the model's predicted and actual values. Smaller MAE and MSE values indicate better predictive performance. The coefficient of determination (R^2) measures how well the predicted values fit the actual data, with values ranging from 0 to 1. A value closer to 1 signifies a higher degree of fit. The formulas for calculating MAE, MSE, and R^2 are as follows:

$$MAE=\frac{1}{N}\sum_{i=1}^{N}\left|y^r{}_i-y^p{}_i\right| \tag{8}$$

$$MSE=\frac{1}{N}\sum_{i=1}^{N}\left(y^p{}_i-y^r{}_i\right)^2 \tag{9}$$

$$R^2=1-\frac{\sum_{i=1}^{N}\left(y^p{}_i-y^r{}_i\right)^2}{\sum_{i=1}^{N}\left(y^r{}_i-\bar{y}_i\right)^2} \tag{10}$$

In the formula, N denotes the sample size,$y^r{}_i$ signifies the i-th actual value, $y^p{}_i$ indicates the i-th predicted value, and $\bar{y}_i$ is the mean of the actual values.

2.4 Numerical Simulation of Dataset Generation

2.4.1 Physical Model

In the present investigation, a two-dimensional numerical model was employed to realize the coupling of flow and electric fields, thereby simulating the dynamic vibration behavior of oil-dispersed droplets under the excitation of chaotic pulse groups electric fields, as illustrated in Figure 3. The deformation ratio D was adopted to quantify the deformation extent of the droplets, where parameter a denotes the droplet deformation along the direction of the electric field, and b denotes the deformation in the direction perpendicular to the electric field.

$$D=\frac{a}{b} \tag{11}$$

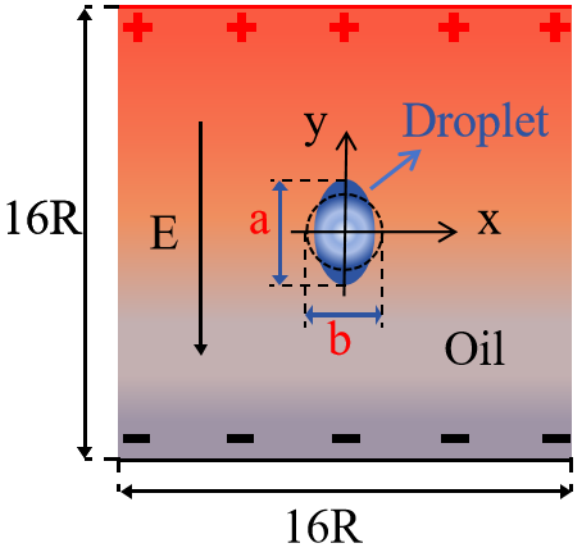

Figure 3 Schematic diagram of the physical model

2.4.2 Chaotic Pulse Group Electric Field

The CPG electric field is based on chaotic pulse width modulation, and the frequency of each group is modulated by the Logistic full mapping. The modulation equation (12) and the iterative equation (13) are as follows[12]:

$$C_{n+1} = 1 - 2C_n^2 \quad (n = 1,2,3\ldots) \qquad (12)$$

$$f_n = \frac{C_n + 1}{2}(f_u - f_l) + f_l \quad (n = 1,2,3\ldots) \qquad (13)$$

where, C_n represents the i-th chaotic iteration value; f_n represents the n-th group of chaotic frequency iteration values; f_u represents the upper limit of frequency; f_l represents the lower limit of chaotic frequency. Assuming that all chaotic pulse groups have the same electric field intensity and the duty cycle (d) remains unchanged, each group contains K pulses, as shown in Figure 4. The expression form of the electric field of the chaotic pulse group is as shown in Equation (14).

$$E(t) = \begin{cases} E, \sum_{i=1}^{n} \frac{k}{f_i} - \frac{1}{f_i}(k+1-j) \le t \le \sum_{i=1}^{n} \frac{k}{f_i} - \frac{1}{f_i}(k+1-j-d) \\ 0, \sum_{i=1}^{n} \frac{k}{f_i} - \frac{1}{f_i}(k+1-j-d) \le t \le \sum_{i=1}^{n} \frac{k}{f_i} - \frac{1}{f_i}(k-j) \end{cases} \quad j = 1,2\ldots k \qquad (14)$$

In the formula, $\boldsymbol{E}$ represents the electric field intensity, f_i represents the i-th set of chaotic frequency iteration values, and j indicates the j-th pulse within each pulse group.

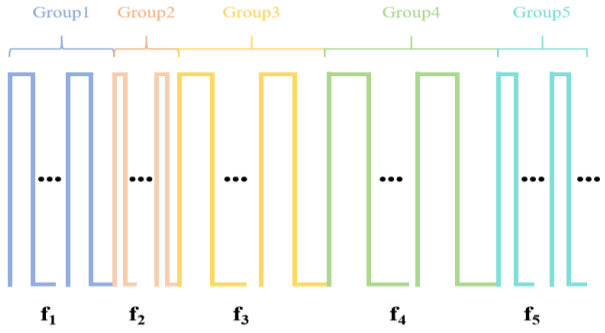

Figure 4 Chaotic pulse group electric field signal

2.4.3 Control Equations

Assume that both the liquid phase and the oil phase are incompressible Newtonian fluids and are immiscible. Due to the small difference in density between oil and water, the influence of gravity can be neglected in the calculation process. The motion between the two phases satisfies the Navier-Stokes equations, as shown below[18,19]:

$$\rho\frac{\partial_u}{\partial_t} + \rho(\boldsymbol{u}\cdot\nabla)\boldsymbol{u} = \nabla\cdot[-p\cdot\boldsymbol{I} + \mu(\nabla\cdot\boldsymbol{u} + (\nabla\cdot\boldsymbol{u})^T)] + \boldsymbol{F_{st}} + \boldsymbol{F_e} + \boldsymbol{F_g} \qquad (15)$$

$$\nabla\cdot\boldsymbol{u} = 0 \qquad (16)$$

Where, $\boldsymbol{u}$ represents the fluid flow velocity (m/s); ρ represents the fluid density (kg/m³); p represents the fluid pressure; $\boldsymbol{I}$ is the identity matrix; μ represents the dynamic viscosity (Pas); $\boldsymbol{F_{st}}$ is the surface tension (N/m); $\boldsymbol{F_e}$ is the electric field force (N); $\boldsymbol{F_g}$ is the gravity (N).

The key to studying the vibration of droplets in oil lies in capturing the changing process at the interface between oil and water. To this end, the Cahn-Hilliard phase field model is used to track the movement and change of the oil-water interface. The Cahn-Hilliard equation is shown in Equation (17)[20].

$$\frac{\partial_\emptyset}{\partial_t} + \boldsymbol{u}\nabla\emptyset = \nabla\cdot\gamma\nabla G \qquad (17)$$

In the formula, $\emptyset$ represents the phase field variable; $\emptyset = 1$ indicates the oil phase; $\emptyset = -1$ indicates the water phase; $\emptyset = 0$ indicates the oil-water interface. Therefore, the distribution of the oil-water two phases can be expressed in terms of volume fraction as:

$$\begin{cases} V_{f_1} = (1-\emptyset)/2 \\ V_{f_2} = (1+\emptyset)/2 \end{cases} \qquad (18)$$

In the equation, V_{f_1} represents the volume fraction of the aqueous phase, V_{f_2} represents the volume fraction of the oil phase, γ represents the migration rate controlling the interface, and H represents the chemical potential energy at the oil-water interface. It is expressed by the following equation:

$$H = \lambda[-\nabla^2\emptyset + \frac{(\emptyset^2-1)\emptyset}{\delta^2}] \qquad (19)$$

In the formula, λ represents the mixed energy density; δ represents the control interface thickness.

In the leakage dielectric model, the dynamic current generated in the current mechanics is very small, and the magnetic effect can be ignored. Therefore, this electric field can be regarded as a non-vortical field ($\nabla \times E = 0$), and it satisfies Maxwell's equations, and the following expression can be obtained[21]:

$$\nabla\cdot(\varepsilon_0\varepsilon_r\boldsymbol{E}) = q_v \qquad (20)$$

Among them, ε_0 represents the vacuum dielectric constant ($\varepsilon_0 = 8.854\times10^{-12}$ F/m); q_v represents the volume charge density; ε_r represents the relative dielectric constant, which is calculated as follows:

$$\varepsilon_r = \varepsilon_{r_1}V_{f_1} + \varepsilon_{r_2}V_{f_2} \qquad (21)$$

In the formula, ε_{r_1} represents the dielectric constant of the aqueous phase; ε_{r_2} represents the dielectric constant of the oil phase. The relationship between the electric field intensity $\boldsymbol{E}$ and the electric field V is expressed as follows:

$$\boldsymbol{E} = -\nabla U \qquad (22)$$

The charge conservation equation can be expressed in the following form:

$$\frac{\partial q_v}{\partial t} + \nabla(k\boldsymbol{E}) = 0 \quad (23)$$

Here, k represents the electrical conductivity of the fluid.

For the leakage model, the time for the redistribution of free charges is much shorter than the time for fluid movement. Therefore, the change in charge over time can be neglected, and the charge equation can be simplified to:

$$\nabla(k\boldsymbol{E}) = 0 \quad (24)$$

Finally, the electric field stress $\boldsymbol{F_e}$ exerted on the droplet can be expressed by the Maxwell stress tensor T.

$$\boldsymbol{F_e} = \nabla \cdot \mathrm{T} \quad (25)$$

For the assumption of incompressible fluids, the Maxwell stress tensor can be expressed as:

$$\mathrm{T} = \varepsilon_r \varepsilon_0 \boldsymbol{EE} - \frac{\varepsilon_r \varepsilon_0 \boldsymbol{EE}}{2} \boldsymbol{I} \quad (26)$$

In the formula, $\boldsymbol{I}$ represents the unit tensor. Therefore, the electric field stress is expressed as:

$$F_e = \nabla \cdot T = q_v \boldsymbol{E} - \frac{1}{2} \nabla \varepsilon_r \varepsilon_0 \boldsymbol{E}^2 \boldsymbol{I} \quad (27)$$

2.4.4 Boundary Conditions

In this work, the COMSOL Multiphysics platform was adopted to realize the coupling of electric and flow fields, and a numerical model targeting incompressible flow was accordingly developed. The Newtonian approach was utilized to accomplish the numerical solution. Within the established model, the oil component was defined as the continuous phase, whereas the liquid droplets acted as the dispersed phase. The thermophysical parameters of the oil and water phases are systematically presented in Table 1. As for the boundary conditions, the upper boundary was assigned with an applied voltage, while the bottom boundary was set to be grounded. The left and right boundaries were configured as open boundaries, serving as the inlet and outlet respectively, with a flow velocity of 0 m/s.

Table 1 Physical property parameters of oil-water two-phase

Medium	Dielectric constant (ε)	Density (ρ) /kg•m^{-3}	Viscosity (μ) /Pa•s	Surface tension coefficient(σ)/ N•m^{-1}
Oil	4.9	0.922×10^3	4.65×10^{-4}	25×10^{-3}
Water	80	1×10^3	1×10^{-3}	

2.4.5 Verification of Grid Independence

This study employs the finite element numerical method to solve and calculate the Navier-Stokes equations, using triangular mesh elements as the basic subdivision units. The grid is densified in the *4R×4R* square core area where the droplet is located, while a relatively sparse grid is set in the non-core area. As the number of grids increases, the occupation of computer hardware resources also increases, prolonging the calculation time. To determine the optimal number of grids suitable for this study, a grid independence verification work was carried out. This study compared the droplet vibrations under different grid numbers, which were 49474, 86856, and 172412. The oil-water physical property parameters are shown in Table 1. The electric field intensity was set at 500 kV/m. The corresponding outcomes are presented in Figure 5. It can be observed from the figure that the vibration response of the droplet excited by the chaotic electric field is notably influenced by the grid quantity. When the number of grids is 49474, the amplitude of the droplet is significantly smaller than that when the grid number is 86856 or 172412. This is because the number of grids is small and the individual grid is large, resulting in a larger calculation error of the numerical model. When the grid number is 86856, the change in the droplet vibration curve is minimal compared to when the grid number is 172412. Therefore, considering the calculation accuracy and resources of the numerical model comprehensively, this study adopted a grid number of 86856 for the subsequent research. The schematic diagram of local grid division is shown in Figure 6. The regular maximum element size is 0.2 mm, the maximum element size in the encrypted area is 0.03 mm, the deformation growth rate is 1.08, and the curvature factor is 0.25.

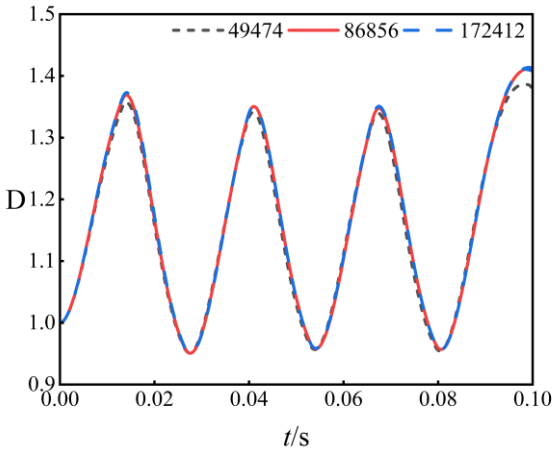

Figure 5 Vibration responses of droplets under different grid quantities

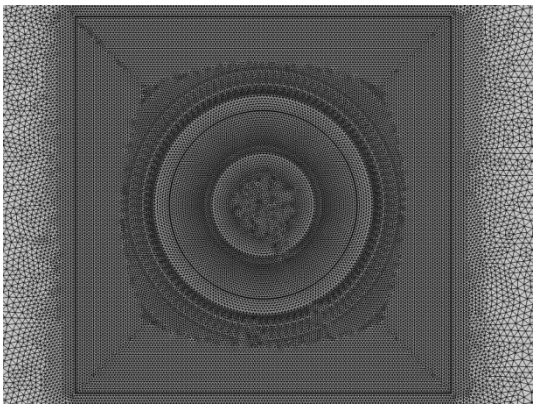

Figure 6 Grid division of the numerical model

3 Results and Discussion

The droplet's vibration response to chaotic pulse group excitation in an electric field was numerically calculated over a 1s duration. To enhance data collection, a sampling

interval of 10^{-4} was employed, resulting in 10001 data points for the dataset. In the numerical model, the electric field intensity was set at 500 kV/m, and the droplet radius was 0.8 mm. The calculation results are shown in Figure 7. As can be seen from the figure, the vibration of the droplet under the chaotic pulse electric field excitation is consistent with the changes of the electric field pulse signal. Since the input parameters of the numerical model are not all evolving over time, the LSTM model proposed in this study takes the chaotic pulse group signal and the time-varying variables as inputs, and takes the deformation degree of the droplet as the target output, thereby achieving the prediction of droplet vibration under chaotic pulse group electric field excitation, breaking the traditional reliance of numerical simulation on the solution of complex control equations, and thus saving computing resources.

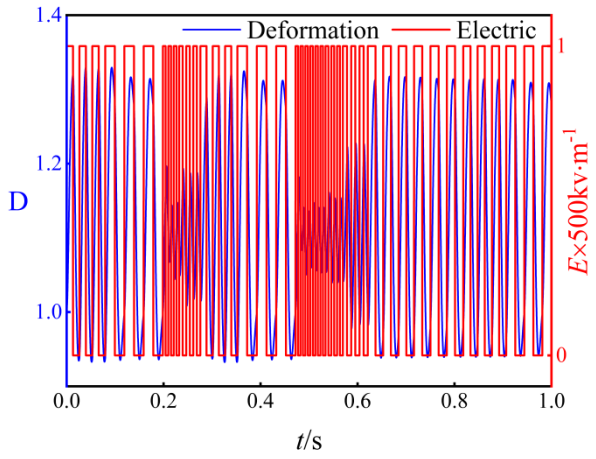

Figure 7 Droplet vibration curve and chaotic pulse group electric field signal

The dataset generated via numerical simulation is partitioned into training, validation, and test subsets with a ratio of 8:1:1.Specifically, the training subset is employed to fit the model, the validation subset is utilized to optimize model performance by means of evaluation indicators, and the test subset is applied to evaluate the predictive capacity of the constructed model. The prediction results of the LSTM model on the test set are shown in Table 2. The LSTM model achieves MSE, MAE,and R^2 values of 4.34×10^{-6}, 0.0017, and 0.99, respectively. These relatively low MSE and MAE values indicate that the error between the predicted values and the actual values is extremely small, which suggests that this model has excellent predictive performance. A higher R^2 indicates a strong fit between actual and predicted values. Therefore, the LSTM model can effectively extract and learn the dependencies within the droplet vibration sequence, capturing the relationship between the droplet vibration sequence and the chaotic pulse group electric field signal as well as the time. Thus, it avoids solving complex control equations and accurately predicts the droplet vibration. Besides, the computational time of the numerical model on the test set is about 1260 seconds, while the time cost for training and parameter optimization of LSTM is roughly 600 seconds. Particularly, the trained LSTM model takes only about 10 seconds to predict in the test set, which is much shorter than the calculation time. This indicates that the LSTM model has great potential for saving computing resources.

To further verify the prediction capability of the LSTM model, comparative analyses were conducted between LSTM and BP, GRU as well as CNN models.The results are shown in Table 2.Compared to BP, GRU, and CNN models, the LSTM model exhibits significantly lower MSE and MAE and a higher R^2. This is because the CNN model and the GRU model merely solve the problem of gradient explosion (gradient vanishing) by controlling information through the gating mechanism and extract important local features of the time series through convolution; the BP model is essentially a feedforward neural network model and is difficult to capture the dynamic feature changes in the sequence. While the LSTM model controls information through the gating mechanism and saves important information of the time series through memory cells. Therefore, compared to the CNN, GRU and BP models, the prediction performance of the LSTM model is better.

Table 2 Test set prediction outcomes of various models

Prediction model	Evaluation indicators	Prediction results
BP	MSE	4.6×10^{-4}
	MAE	0.0183
	R^2	0.9788
GRU	MSE	3.1×10^{-4}
	MAE	0.0139
	R^2	0.985
CNN	MSE	2.5×10^{-4}
	MAE	0.0125
	R^2	0.988
LSTM	MSE	4.34×10^{-6}
	MAE	0.0017
	R^2	0.99

4 Conclusion

The concept of chaotic pulse group electric field was proposed to overcome the oil-water separation step in the existing waste oil resource utilization processes. However, current numerical methods for analyzing droplet vibrations under chaotic pulse group electric field excitation involve complex parameters, which demand significant computational resources and time, yielding only limited data. To address this, further analysis and research were conducted. A neural network approach was proposed, specifically constructing a droplet vibration prediction model using LSTM. The results show that LSTM can effectively capture the long-term correlations of the droplet vibration sequence and accurately predict the droplet vibration under the excitation of chaotic pulse groups, while saving computing resources. Furthermore, compared to BP, GRU, and CNN models, the LSTM model exhibits superior predictive performance.

Acknowledgements

This work was partially supported by grants from the National Natural Science Foundation of China (Grant No.

22178036 and No.52404115), CSTC projects (Grant CSTB2024NSCQ-LZX0021, CSTB2024TIAD-KPX0070, CSTB2023NSCQ-MSX0791 and CSTB2023NSCQ-LZX0096), projects of science and technology research program of Chongqing Education Commission of China (Grant No. KJZD-M202200801, KJZD-M202300802 and CXQT21023).

References

1. Tianpeng Li , Tiezhu Wang, Jie Yang . Application status and prospects of waste lubricating oil regeneration processes at home and abroad[J]. Chemical Engineer, 2025, 39(03):64-68+72
2. Yali Ma, Yanjie Tong, Shubin Mi. Study on Recovery and Recycling and Utilization of Waste Lubricating Oil[J]. Modern Chemical Researc, 2020, (23): 100-101.
3. Xinhe Zhuang. Technical Progress of Disposal and Resource Utilization of Industrial Hazardous Wastes[J]. Total Corrosion Control, 2025, 39(01): 202-204.
4. Yangyang Liang, Jinhui Li, Qingyin Dong, et al. Present situation and prospect of used lubricating oil recycling technology and management in China[J]. Journal of Environmental Engineering Technology, 2018, 8(3) : 282-289.
5. Reza Zolfaghari, Ahmadun Fakhru' l-Razi, Luqman C. Abdullah, et al. Demulsification techniques of water-in-oil and oil-in-water emulsions in petroleum industry [J]. Separation and Purification Technology, 2016, 170: 377-407.
6. Huiling Huang, Yan Li, Chao Huang, et al. A review of stimuli-responsive microemulsions: Responsive mechanism, physicochemical property, and application[J]. Journal of Molecular Liquids, 2024, 401: 124666.
7. Yuling Lyu, Yueyang Wu, Miqi Niu, et al. Deformation and vibration of droplet in oil subjected to a chaotic-pulse-width-modulation electric field[J]. Journal of Molecular Liquids, 2023, 390(B): 123102.
8. Tao Liu, Bauyrzhan Sarsenbekuly, Wanli Kang. Breakdown mechanism and application of high frequency pulsed electric field-demulsifier combination on water-in-oil emulsion[J]. Colloids and Surfaces A: Physicochemical and Engineering Aspect, 2025, 707: 135846.
9. Wenjun Zhou, Shunan Cao, Shuibing Liu. Mechanism of Water Removal from Petroleum by High Voltage Pulse[J]. High Voltage Engineering, 1995, (02):24-26.
10. Li B, Fan Y, Sun Z, et al. Effects of high-frequency pulsed electrical field and operating parameters on dehydration of SAGD produced ultra-heavy oil[J]. Powder Technology, 2017, 316: 338-344.
11. Jian Zhang, Shouping Shou, Qinrong Gan. Dynamic model of liquid droplets of water-in-oil emulsions with high frequency pulsating electrical field[J]. CIESC Journal, 2007(04): 875-880.
12. Peng Y, Liao Z, Zhang Y, et al. Analysis of deformation dynamics of droplet in oil under the CPG electric field[J]. Chemical Engineering Research and Design, 2022, 183: 357-367
13. Seyed Reza ASADOLAHPOUR, Zeyun JIANG, Helen LEWIS, et al. Deep learning for pore-scale two-phase flow: Modelling drainage in realistic porous media[J]. Petroleum Exploration and Development, 2024, 51(5): 1301-1315.
14. Shengpeng Xiao, Chuyi Wan, Hongbo Zhu, et al. Deep learning-based reconstruction of three-dimensional particle volume fraction fields in solid-liquid two-phase pipe flow from single cross-sectional data[J]. Powder Technology, 2026, 468: 121616.
15. Geethal Siriwardana, Anjan Rajapakse, Thilaksiri Bandara, et al. Multiclass classification of two-phase flow patterns using classical and deep learning models with automated hyperparameter optimization[J]. International Communications in Heat and Mass Transfer, 2025, 269(D): 109886.
16. Xiao Wang, Pingsong Zhang, Chang Liu. Acoustic signal-based identification of pipeline defects using optimized MFCC and LSTM[J]. Journal of Pipeline Science and Engineering, 2025, 100355.
17. Chenkai Li, Donge Zhao, Bin Zhang, et al. Research on a fast signal recognition method for a laser screen measurement system based on LSTM[J]. Measurement, 2025, 254:117905.
18. Mandal S, Bandopadhyay A, Chakraborty S. The effect of uniform electric field on the cross-stream migration of a drop in plane Poiseuille flow. Journal of Fluid Mechanics. 2016;809:726-774.
19. López-Herrera J M, Popinet S, Herrada M A. A charge-conservative approach for simulating electrohydrodynamic two-phase flows using volume-of-fluid[J]. Journal of Computational Physics, 2011,230(5):1939-1955.
20. FENG J J, LIU C, SHEN J, et al. A diffuse-interface method for simulating two-phase flows of complex fluids[J]. Journal of Fluid Mechanics, 2004,515:293-317.
21. Tomar G, Gerlach D, Biswas G, et al. Two-phase electrohydrodynamic simulations using a volume-of-fluid approach[J]. Journal of Computational Physics, 2007,227(2):1267-1285.